Mobility Modes for Pulse-Shaped OTFS with Linear Equalizer

Andreas Pfadler*†, Peter Jung† and Slawomir Stanczak†
*Group Innovation, Volkswagen AG, Wolfsburg, Germany
andreas.pfadler@volkswagen.de
†Fraunhofer Heinrich Hertz Institute and Technical University of Berlin, Berlin, Germany
{peter.jung,slawomir.stanczak}@hhi.fraunhofer.de

***Abstract*—Orthogonal time frequency and space (OTFS) modulation is a pulse-shaped Gabor signaling scheme with additional time-frequency (TF) spreading using the symplectic finite Fourier transform (SFFT). With a sufficient amount of accurate channel information and sophisticated equalizers, it promises performance gains in terms of robustness for high mobility users. To fully exploit diversity in OTFS, the 2D-deconvolution implemented by a linear equalizer should approximately invert the doubly dispersive channel operation, which however is a twisted convolution. In theory, this is achieved in a first step by matching the TF grid and the Gabor synthesis and analysis pulses to the delay and Doppler spread of the channel. However, in practice, one always has to balance between supporting high granularity in delay-Doppler (DD) spread, and multi-user and network aspects.**

In this paper, we propose *mobility modes* with distinct grid and pulse matching for different doubly dispersive channels. To account for remaining self-interference, we tune the minimum mean square error (MMSE) linear equalizer without the need of estimating channel cross-talk coefficients. We evaluate our approach with the QuaDRiGa channel simulator and with OTFS transceiver architecture based on a polyphase implementation for orthogonalized Gaussian pulses. In addition, we compare OTFS to a IEEE 802.11p compliant design of cyclic prefix (CP) based orthogonal frequency-division multiplexing (OFDM). Our results indicate that with an appropriate *mobility mode*, the potential OTFS gains can be indeed achieved with linear equalizers to significantly outperform OFDM.

I. Introduction

Strict requirements on reliability and efficiency in high mobility communication scenarios, such as vehicle-to-everything (V2X) communication, are pushing legacy systems to their limits. Orthogonal frequency-division multiplexing (OFDM) is a widely-used modulation scheme which however suffers substantial performance degradation and inflexibility in scenarios with high Doppler spreads [1]. Consequently, there is a need for the development of novel modulation schemes that are flexible, efficient and robust in doubly dispersive channels.

An orthogonal time frequency and space (OTFS) waveform is introduced by Hadani *et. al* [2] as a promising combination of classical pulse-shaped Weyl-Heisenberg (or Gabor) multicarrier schemes with a distinct time-frequency (TF) spreading. Data symbols are spread with the symplectic finite Fourier transform (SFFT) over the whole TF grid. This particular linear pre-coding accounts for the doubly dispersive nature of time-varying multipath channels seen as linear combinations of TF shifts. Several studies show that OTFS outperforms OFDM in such situations [3], [4], [5]. Another research work focuses on a performance comparison of OFDM, generalized frequency division multiplexing (GFDM), and OTFS [6]. It reveals significant advantages of OTFS in terms of bit error rate (BER) and frame error rate (FER) in relation to the others. However, so far research has mainly focused on OTFS with the assumption of perfect grid matching and often with idealized pulses, violating the uncertainty principle. In many cases, ideal channel knowledge is assumed, including the cross-talk channel coefficients.

Different doubly dispersive communication channels provide distinct delay-Doppler (DD) spread and diversity characteristics. Particular single dispersive cases therein are time or frequency-invariant channels, which boil down to simple frequency or time division communication schemes, respectively. For some high mobility scenarios, the channel becomes dispersive in both time and frequency domain. Especially, V2X channels differ in their dissipation in both domains. Depending on the communication scenario, a distinct spreading region is spanned: $U := [0, \frac{\tau}{B}] \times [-\frac{\nu B}{L}, \frac{\nu B}{L}]$, where B, L, ν, and τ are the bandwidth, signal length, Doppler, and delay spread, respectively. In order to cope with doubly dispersive channels, the synthesis pulse used at the transmitter, the analysis pulse used at the receiver, and their TF grid need to match U [7], [8], [9]. A common way is to design the ratio of time and frequency shifts T and F as well as TF spreads σ_t and σ_f of the Gabor pulses with respect to the channel scattering function under the wide-sense stationary uncorrelated scattering (WSSUS) assumption:

$$\frac{T}{F} = \frac{\sigma_t}{\sigma_f} \stackrel{!}{=} \frac{\tau_{max}}{2\nu_{\max}} \tag{1}$$

where $\frac{\tau_{max}}{2\nu_{\max}}$ is the ratio between the maxima of the delay and the Doppler spread of the channel. This approach is referred as pulse and grid matching [7], [10], [8], [9]. With the goal of satisfying the condition of pulse and grid matching in (1), we propose and investigate distinct *mobility modes*.

For coherent communication, one needs to estimate the doubly dispersive channel operation and invert it at the receiver. In general, linear equalizer are favored for channel equalization, since they have a lower complexity compared to e.g. maximum-likelihood equalizer (MLE) or iterative techniques such as interference cancellation [11]. Although MLE enjoys the maximum diversity, in some cases linear equalizer can achieve the same diversity gain as MLE [12], for example in the case of non-singular convolutions. In [13], it has

been observed that in most cases full OTFS diversity is not achieved when using a common minimum mean square error (MMSE) equalization. On the contrary, MLE or interference cancellation techniques for OTFS are complex and also require accurate estimation of the cross-talk channel coefficients. Indeed, the remaining self-interference caused by suboptimal pulse and grid matching needs to be estimated and taken into account at the equalizer. In our previous work, we proposed a linear equalizer which accounts for self-interference on a frame base [14]. This approach is used in the presented work to account for the remaining self-interference.

In this paper, we propose *mobility modes* that control the self-interference on a coarse level and to instantaneously tune the linear MMSE equalizer by estimating from pilot and guard symbols the remaining self-interference power. The main contributions of this paper can be summarized as follows:

- we study OTFS from the perspective of the pulse-shaped Gabor signaling with additional TF spreading, implemented using the MATLAB toolbox LTFAT [15],
- we consider doubly dispersive vehicular channels in a concrete geometry-based scenario generated by the QuaDRiGa channel simulator [16] using pilot-based channel estimation as in [17],
- we propose *mobility modes* with distinct pulse and grid matching, and
- we take into account the impact of the remaining self-interference in the equalizer due to imperfect 2D-deconvolution of the twisted convolution affected by grid and pulse mismatch [14].

II. OTFS System Model

In this section, we introduce the system model and the OTFS transceiver structure. OTFS is a combination of classical pulse shaped multicarrier transmission with Gabor structure, i.e., TF translations on a regular grid in the TF plane, and additional TF spreading using the SFFT.

A. Time-Frequency Grid and Pulse Shaping

The frequency resolution is $F = \frac{B}{M}$, where B is the overall bandwidth and M the number of subcarriers. The time resolution is $T = \frac{D}{N}$, with D being the frame duration and N the number of time symbols. The TF grid is sampled with T and F period in the time and frequency domain, respectively. The filterbank length also depends on the dimensioning of the used synthesis and analysis pulse and the so-called time frequency product $T \cdot F$. The Gabor filterbanks at the transmitter and at the receiver are configured with pulses γ for the synthesis and g for the analysis of the signals, respectively. Three cases are distinguished: $TF > 1$, $TF = 1$, and $TF < 1$ – sometimes referred to as undersampling, critical sampling, and oversampling of the TF plane, respectively [18]. Throughout this paper, we assume $TF = 1.25$, as it is a typical compromise between maximizing the signal to interference ratio (SIR) and the loss in degrees of freedom [19]. To guarantee perfect reconstruction in the non-dispersive and noiseless case, we require that the pulses γ and g are biorthogonal:

$$\langle \gamma, g_{nT,mF} \rangle = \delta(m)\delta(n) \tag{2}$$

where we define $g_{\alpha,\beta}(t) = g(t-\alpha)e^{j2\pi\beta t}$ (same for $\gamma_{\alpha,\beta}(t)$) with $\delta(0) = 1$ and zero otherwise. Here, we use $\langle u, v \rangle = \int u(t)^* v(t) dt$ as inner product on $L_2(\mathbb{R})$, the Hilbert space of signals with finite energy. To ensure uncorrelated noise contributions, we assume the synthesis and analysis pulses to be equal, resulting in an orthogonal pulse. Given a preliminary prototype pulse we use the well-known $S^{-1/2}$-trick to perform the orthogonalization, i.e. constructing a tight Gabor frame on an adjoint lattice [9]. However, exact orthogonality at the output of doubly dispersive channels is usually destroyed resulting in self-interference. By choosing different pulses for the transmitter and receiver, it may even be possible to further reduce the self-interference for classes of doubly dispersive channels.

B. TF-Spreading and De-Spreading

The transceiver structure is essentially the same as in many pulse shaped multicarrier schemes, like pulse-shaped OFDM, biorthogonal frequency division multiplexing (BFDM) or filter bank multicarrier (FBMC). A distinct feature of OTFS is the spreading. All symbols $X = \{X_{lk}\}_{(l,k)\in\mathcal{I}}$, with $\mathcal{I} \subseteq [M] \times [N]$, are pre-coded with the inverse SFFT denoted as $\mathcal{F}_s^{-1}$. The SFFT differs from the ordinary 2D Fourier transformation by its sign switching in the exponent and coordinates swapping. One can interpret this by mapping an array of discrete DD positions (l, k) to an array of grid points (m, n) in the TF plane, since time shifts lead to oscillations in frequency and frequency shifts result in oscillations in time. More precisely, at the transmitter, the pre-coding is given by $x = \mathcal{F}_s^{-1} X = \{x_{mn}\}_{(m,n)\in\mathcal{I}}$ where

$$x_{mn} = \frac{1}{\sqrt{NM}} \sum_{(l,k)\in\mathcal{I}} X_{lk} e^{j2\pi(\frac{nk}{N} - \frac{ml}{M})}. \tag{3}$$

The received and equalized symbols $\hat{y} = \{\hat{y}_{mn}\}_{(m,n)\in\mathcal{I}}$ in the TF plane are de-spreaded again as $\hat{Y} = \mathcal{F}_s \hat{y}$ such that

$$\hat{Y}_{lk} = \frac{1}{\sqrt{NM}} \sum_{(m,n)\in\mathcal{I}} \hat{y}_{mn} e^{-j2\pi(\frac{nk}{N} - \frac{ml}{M})}. \tag{4}$$

C. Structure of the OTFS Frames

We use a pilot-based channel estimation, where a pilot is inserted in the DD domain as proposed by [17]. The pilot is sent by the transmitter in the same frame as the data. In doing so, the channel can be easily estimated at the receiver in the DD domain. The symbols to be placed in the DD domain are threefold. The data symbols, usually coming from a particular modulation alphabet, are placed on positions indexed by the set $\mathcal{D} \subset \mathcal{I}$. Positions used for channel estimation are defined by the set $\mathcal{P} \subset \mathcal{I}$, with $\mathcal{D} \cap \mathcal{P} = \emptyset$, which will contain a single pilot symbol; the other positions are unused and can be seen as guard symbols. We assume that

$$\mathcal{P} = \{\, (l,k) : l \in [2W], k \in [4Q] \,\} \subset \mathcal{I}, \tag{5}$$

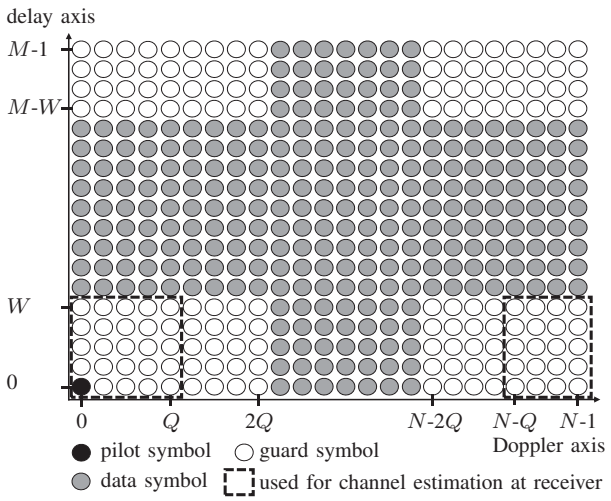

Fig. 1. Exemplary OTFS frame in the DD domain.

where W and Q define the guard region in delay and Doppler domain, respectively. We use an arbitrary location $[l = \tau, k = 2\nu]$ for the non-zero pilot symbol. Note that W and Q need to be defined with respect to the expected DD shift [20]. Fig. 1 depicts an example of an OTFS frame with data, pilot, and guard symbols. We choose Q and W with an appropriate dimension for each OTFS mode. We assume a constant product of $Q \cdot W$, i.e. 1024 symbols, to compare different configurations with the same pilot overhead (same data rate). For simplicity, we set the non-zero pilot $X_{lk} = \sqrt{P_p}$ at $k = 0$ and $l = 0$ with the normalized power of $P_p = 2Q4W$ and all the other symbols in $\mathcal{P}$ are zero-valued guard symbols.

D. Gabor Synthesis Filterbank

The OTFS frame in the TF plane is then used to synthesize a transmit signal $s(t)$. This is implemented with a Gabor synthesis filterbank configured with a transmit pulse γ [7]. We can formally write this as

$$s(t) = \sum_{(m,n)\in\mathcal{I}} \gamma(t - nT)e^{j2\pi mFt}x_{mn}, \qquad t \in \mathbb{R}. \tag{6}$$

E. The Doubly Dispersive Channel

For a doubly dispersive channel, the noiseless time-continuous channel output consists of an unknown linear combination of TF translates of the input signal $s(t)$. We can formally express this operation as

$$\begin{aligned} r(t) &= \sum_{p=1}^{p_{\max}} h_p(t)s(t - \tau_p) \\ &= \sum_{(m,n)\in\mathcal{I}} x_{mn} \sum_{p=1}^{p_{\max}} h_p(t)\gamma(t - \tau_p - nT)e^{j2\pi mF(t-\tau_p)}, \end{aligned} \tag{7}$$

where the pth discrete propagation path has the delay τ_p for $p = 1 \dots p_{\max}$. Let us also define the index set $\mathcal{A} := [1 \dots d_{\max}] \times [1 \dots p_{\max}]$. For $p \in \{1, p_{\max}\}$, $h_p(t)$ is then given by

$$h_p(t) = \sum_{d=1}^{d_{\max}} S_{dp}e^{j2\pi t\nu_d}, \tag{8}$$

where $\{S_{dp}\}_{(d,p)\in\mathcal{A}}$ can be seen as the discrete DD spreading function [21]. In particular, this simplified model implies that each path has the same range of frequency shifts $\{\nu_d\}_{d=1}^{d_{\max}}$ but with possibly different coefficients. We assume that the set of TF shifts $\{(\nu_d, \tau_p)\}_{(d,p)\in A} \subset U$ are usually in a box $U := [-\nu_{\max}, \nu_{\max}] \times [0, \tau_{\max}]$ of size $|U| = 2\nu_{\max}\tau_{\max} \ll 1$, which is also known as the *underspread assumption*. Putting (6) in (7) with (8) yields

$$\begin{aligned} r(t) = \sum_{(m,n)\in\mathcal{I}} x_{mn} \sum_{(d,p)\in\mathcal{A}} S_{dp}\gamma(t - \tau_p - nT) \\ \times e^{j2\pi mF(t-\tau_p)}e^{j2\pi t\nu_d}. \end{aligned} \tag{9}$$

F. Gabor Analysis Filterbank

The received signal is down-converted and passed through an analysis filterbank. The output of the noiseless Gabor analysis filterbank in TF slot $(\bar{m}, \bar{n}) \in \mathcal{I}$ is then

$$\begin{aligned} y_{\bar{m}\bar{n}} &= \langle g_{\bar{n}T,\bar{m}F}, r\rangle \\ &= \sum_{(m,n)\in\mathcal{I}} x_{mn} \sum_{(d,p)\in\mathcal{A}} S_{dp}e^{-j2\pi mF\tau_p} \\ &\quad \times \langle g_{\bar{n}T,\bar{m}F}, \gamma_{\tau_p+nT,\nu_d+mF}\rangle. \end{aligned} \tag{10}$$

III. Channel estimation and self-interference

In this section, we explain in more details, the channel estimation, the equalization and the amount of self-interference which remains in the OTFS transceiver structure. In particular, we show the link between the equalization as a 2D-deconvolution and the true channel mapping, given as a twisted convolution.

A. Impact of the Self-Interference

To reveal the impact of pulse and grid mismatch on self-interference, we rewrite the inner product in (10) and compute it separately:

$$\begin{aligned} &\langle g_{\bar{n}T,\bar{m}F}, \gamma_{\tau_p+nT,\nu_d+mF}\rangle = \langle g_{\bar{n}T,0}, \gamma_{\tau_p+nT,[m-\bar{m}]F+\nu_d}\rangle \\ &= e^{j2\pi([m-\bar{m}]F+\nu_d)\bar{n}T}\langle g_{\bar{n}T,0}, \gamma_{\tau_p+nT+[\bar{n}-n]T,[m-\bar{m}]F+\nu_d}\rangle \\ &= e^{j2\pi([m-\bar{m}]F+\nu_d)\bar{n}T}A([n-\bar{n}]T + \tau_p, [m-\bar{m}]F + \nu_d), \end{aligned} \tag{11}$$

where $A(\alpha, \beta) = \langle g, \gamma_{\alpha,\beta}\rangle$ is the cross-ambiguity function. The goal is to design the pulses γ and g such that

$$\begin{aligned} &A([n-\bar{n}]T + \tau_p, [m-\bar{m}]F + \nu_d) \\ &\approx \delta(n-\bar{n})\delta(m-\bar{m})A(\tau_p, \nu_d), \end{aligned} \tag{12}$$

for all values $(\tau_p, \nu_d) \in U \neq 0$. Roughly speaking, this implies that $\mathbb{E}(|z_{\bar{m}\bar{n}}|^2)$ (taken over data symbols and channel realizations) of the self-interference $z_{\bar{m}\bar{n}}$, defined to be

$$\begin{aligned} z_{\bar{m}\bar{n}} := \sum_{(m,n)\neq(\bar{m},\bar{n})} x_{mn}S_{dp}e^{-j2\pi(\bar{m}F\tau_p - \bar{n}T\nu_d - [m-\bar{m}]F\bar{n}T)} \\ A([n-\bar{n}]T + \tau_p, [m-\bar{m}]F + \nu_d), \end{aligned} \tag{13}$$

TABLE I
OVERVIEW OF THE INVESTIGATED MOBILITY MODES

Mode	N	M	T	F	T/F
OFDM	64	64	0.125 μs	156.25 kHz	8e-13
I	64	64	0.125 μs	156.25 kHz	8e-13
II	32	128	0.5 μs	79.125 kHz	6.4e-12
III	128	32	31.25 ns	312.5 kHz	1e-13
IV	16	256	2 μs	39.063 kHz	5.12e-11
V	256	16	62.5 ns	625 kHz	1.25e-14
VI	8	512	8 μs	19.531 kHz	4.096e-10
VII	512	8	1.953 ns	1250 kHz	1,5625e-15

becomes negligibly small. Note that $\mathbb{E}(|z_{\bar{m}\bar{n}}|^2) > 0$ since pulses g and γ such that $A_{g\gamma}(\alpha,\beta) = A_{g\gamma}(0)\delta(\alpha)\delta(\beta)$ for all the (α,β) do not exist. Therefore, the goal of matched pulse shaping is instead to minimize the expected self-interference power.

By considering self-interference in the system model we obtain

$$y_{\bar{m}\bar{n}} = x_{\bar{m}\bar{n}} \overbrace{\sum_{(d,p)\in\mathcal{A}} S_{dp} \cdot A_{g\gamma}(\tau,\nu) e^{-j2\pi(\bar{m}F\tau_p - \bar{n}T\nu_d)}}^{h_{\bar{m}\bar{n}}} + z_{\bar{m}\bar{n}}. \tag{14}$$

Applying $\mathcal{F}_s$ to (14) shows that in the first order (up to inference) the channel acts as 2D-convolution since

$$\begin{aligned} Y_{\bar{l}\,\bar{k}} &= \frac{1}{\sqrt{NM}} \sum_{(\bar{m},\bar{n})\in\mathcal{I}} y_{\bar{m}\bar{n}} e^{-j2\pi(\frac{\bar{n}\bar{k}}{N} - \frac{\bar{m}\bar{l}}{M})} \\ &= \frac{1}{\sqrt{NM}} \sum_{(\bar{m},\bar{n})\in\mathcal{I}} \left(h_{\bar{m}\bar{n}} x_{\bar{m}\bar{n}} + z_{\bar{m}\bar{n}}\right) e^{-j2\pi(\frac{\bar{n}\bar{k}}{N} - \frac{\bar{m}\bar{l}}{M})} \\ &=: \frac{1}{\sqrt{NM}} \sum_{(\bar{m},\bar{n})\in\mathcal{I}} \left(h_{\bar{m}\bar{n}} x_{\bar{m}\bar{n}}\right) e^{-j2\pi(\frac{\bar{n}\bar{k}}{N} - \frac{\bar{m}\bar{l}}{M})} + Z_{\bar{l}\bar{k}}. \end{aligned} \tag{15}$$

As point-wise multiplication in the TF plane is (circular) 2D-convolution in the DD plane, we can finally write

$$Y_{\bar{l}\,\bar{k}} = \sqrt{NM}(H * X)_{\bar{l}\bar{k}} + Z_{\bar{l}\bar{k}}, \tag{16}$$

where $H = \mathcal{F}_s h$ is the channel transfer function. The magnitude of $Z_{\bar{l}\bar{k}}$ is depending on the matching given in (12), i.e. the higher the mismatch the larger the self-interference.

B. Delay-Doppler Channel Estimation

We estimate the channel with the pilot sent by the transmitter in the DD domain. The $\mathcal{F}_s^{-1}$ is applied to quarter of the guard area, where the channel impulse response (CIR) is obtained by [20]:

$$\hat{h}_{\bar{m}\bar{n}} = \frac{1}{\sqrt{NM}} \sum_{\bar{l}=0,\bar{k}=N-Q}^{\bar{l}=W,\bar{k}=2Q} Y_{\bar{l}\bar{k}} e^{j2\pi(\frac{\bar{n}\bar{k}}{N} - \frac{\bar{m}\bar{l}}{M})}, \tag{17}$$

for all $(\bar{m},\bar{n}) \in \mathcal{I}$. Fig. 1 highlights the symbols used for channel estimation in a black dashed frame. The remaining guard symbols (outside the black dashed frame) are needed to avoid interference between the pilot and data symbols.

TABLE II
SIMULATION AND SYSTEM PARAMETERS

Parameter	Notation	Values	Unit
Carrier frequency	f_c	5.9	GHz
Bandwidth	B	10	MHz
Modulation scheme	QPSK	-	-
TF product	TF	1.25	-
Cyclic prefix	CP	16	-
Filter length	L	5120	-
OTFS pilot and guard symbols	QW	1024	-
OFDM pilots	O	1024	-
FEC Coding (soft-decision)	convolutional code	-	-
Code rate	r	0.5	-
Channel model V2I	3GPP 38.901	-	-
Channel model V2V	QuaDRIGa UD2D	-	-

C. Time-Frequency Equalization

We propose to use *mobility modes* to achieve sufficient performance at moderate complexity. The appropriate *mobility mode* controls the self-interference on a coarse level. In addition, we tune the MMSE equalizer to account for the remaining self-interference power. The received frame (14) is equalized with the estimated channel (17) by MMSE equalization:

$$\hat{y}_{\bar{m}\bar{n}} = \frac{\hat{h}^*_{\bar{m}\bar{n}}\, y_{\bar{m}\bar{n}}}{|\hat{h}_{\bar{m}\bar{n}}|^2 + \sigma^2 + \underbrace{\mathbb{E}\{|z_{\bar{m}\bar{n}}|^2 + |h_{\bar{m}\bar{n}} - \hat{h}_{\bar{m}\bar{n}}|^2\}}_{I}}, \tag{18}$$

where σ^2 is the noise variance. Therefore, it is essential to estimate the mean self-interference power I, which contains the averaged power of the self-interference and the error of the channel estimation at the receiver. We approach this by estimating I as the empirical mean (over $(\bar{m},\bar{n})$) from pilot and guard symbols for each frame to tune the MMSE equalizer instantaneously to the corresponding channel realization. For a given I, the equalized symbols in the DD domain are given by:

$$\hat{Y}_{\bar{l}\,\bar{k}}(I) = \frac{1}{\sqrt{NM}} \sum_{(\bar{m},\bar{n})\in\mathcal{I}} \frac{\hat{h}^*_{\bar{m}\bar{n}}\, y_{\bar{m}\bar{n}}}{|\hat{h}_{\bar{m}\bar{n}}|^2 + \sigma^2 + I} e^{-j2\pi(\frac{\bar{n}\bar{k}}{N} - \frac{\bar{m}\bar{l}}{M})}. \tag{19}$$

An intuitive approach is then to minimize a given error metric $d(\cdot,\cdot)$ between the transmitted (assumed to be known at receiver) and equalized pilot and guard symbols, $X_{\bar{l}\,\bar{k}}$ and $\hat{Y}_{\bar{l}\,\bar{k}}$, respectively, as proposed in [14]:

$$I_{\text{opt}} = \underset{I\geq 0}{\operatorname{argmin}} \sum_{(\bar{k},\bar{l})\in\mathcal{P}} d(\hat{Y}_{\bar{l}\,\bar{k}}(I), X_{\bar{l}\,\bar{k}}). \tag{20}$$

As error metric $d(a,b) \sim \|a-b\|_2$, we use the ℓ_2–norm on a finite grid as in [14]. Finally, each frame is then equalized with its individual I_{opt}.

IV. MOBILITY MODES

In this section, we introduce the *mobility modes* to reduce the self-interference caused by grid and pulse mismatches. Coping with different channel conditions, i.e. distinct delay and Doppler spreads, we investigate seven different *mobility*

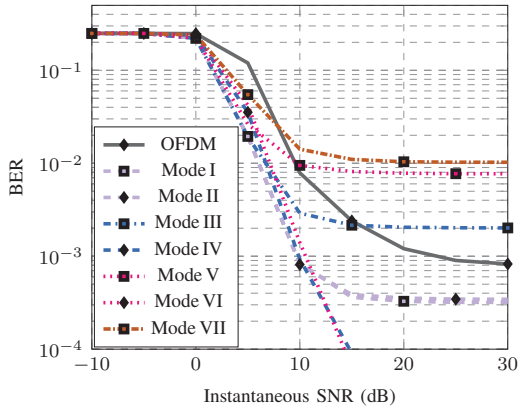

(a) V2I with $\Delta v = 50\,^{km}/_{h}$

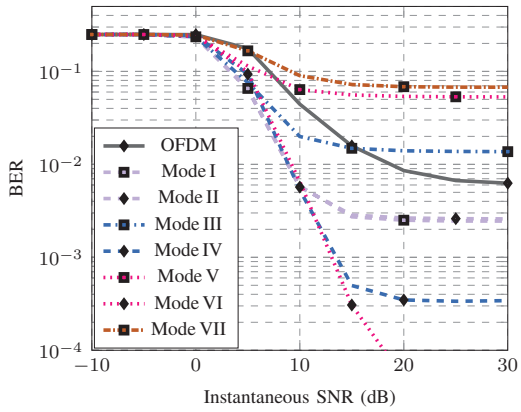

(b) V2I NLOS with $\Delta v = 50\,^{km}/_{h}$

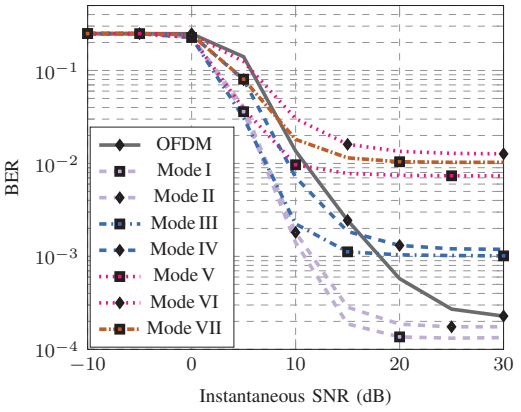

(c) V2V with $\Delta v = 160\,^{km}/_{h}$

Fig. 2. BER for distinct V2X scenarios and different *mobility modes*. We use the QuaDRIGa channel simulator [16] with the 3GPP 38.901 and QuaDRIGa UD2D channel model for V2I and V2V scenarios, respectively. The convolution coding is using a code rate of $r = 0.5$.

modes. The *mobility mode* needs to be defined by the long-term expectation of the channel. The proposed *mobility modes* are aiming to yield a small deviation from equality in (12) and hence to reduce the impact of self-interference. The remaining self-interference power is then estimated in (20) and used for the linear equalization. Table I presents the *mobility modes* I to XII. The higher the resolution in time (N symbols), the fewer resolution in frequency domain (M subcarrier) and vice versa. Mode I represents the case for equal time and frequency resolution. Each *mobility mode* therefore has its own pulse shape which is achieved by squeezing and orthogonalization according to the procedure explained in the introduction. We assume that the transmitter and the receiver use the same mode. The appropriate mode can be selected depending on the second order statistic of the channel. The selection of an appropriated mode is left for future work.

V. Numerical Results

In this section, we numerically analyze the approach of using distinct *mobility modes* for grid and pulse matching. Table II summarizes the parameters used to obtain the numerical results. In the case of cyclic prefix (CP) based OFDM, we follow the regularized least-squares approach for channel estimation and use zero-forcing equalization [22]. We study one OFDM configuration, with the same TF grid as OTFS Mode I (see Table I). The OFDM configuration is close to the 802.11p standard where the rectangular pulses include the CP. We present the coded BER curves for different communication scenarios for all modes, where convolution codes with a code rate of $r = 0.5$ are used. Table III lists all modes and the corresponding signal to noise ratio (SNR) needed to reach the target BER of 10^{-2} and 10^{-3}. The best mode with the lowest SNR is highlighted in blue. We also list the lowest BER reached for each mode. Fig. 2a and 2b depict the BER for the vehicle-to-infrastructure (V2I) scenario under line-of-sight (LOS) and strict non line-of-sight (NLOS) condition, respectively. Each V2X scenario is characterized by a distinct DD spread. Therefore, for each case, a different *moblity mode* is appropriate, i.e. Mode I or II in LOS and Mode VI or IV in NLOS. In Fig. 2c, we present a vehicle-to-vehicle (V2V) scenario with a relative speed of $\Delta v = 160\,^{km}/_{h}$. Here Mode I outperforms the others. In general, it can be observed that OTFS outperforms OFDM with an appropriate *mobility mode* in all scenarios.

VI. Conclusions

We introduced *mobility modes* for pulse-shaped OTFS modulation to enable linear equalization. By selecting an appropriate *mobility mode* for pulse and grid matching the self-interference level, immanent in doubly dispersive channels, reduces and hence, also the BER. It can be concluded that through the introduction of *mobility modes*, one can improve the system performance for low-complexity equalizers implementing tuned 2D-deconvolutions instead of dealing with the full twisted convolution. We also point out that the tuning of the equalizer for the remaining interference levels provides further gains of the *mobility modes*. For each V2X scenario a distinct *mobility mode* outperforms the others and the effect improves with more accurate channel knowledge. In all scenarios at least one OTFS mode outperforms the CP-based OFDM. We have shown the importance of the selection of an appropriate mobility mode.

TABLE III
OVERVIEW OF MOBILITY MODES FOR DIFFERENT V2X SCENARIOS AND MINIMUM SNR NEEDED TO REACH THE TARGET BER OF 10^{-2} AND 10^{-3}.

V2X scenario	Target BER	OFDM	Mode I	Mode II	Mode III	Mode IV	Mode V	Mode VI	Mode VII
V2I $\Delta v = 10\,km/h$	10^{-2}	9.9 dB	7.3 dB	**7.1 dB**	7.7 dB	8.3 dB	9.7 dB	8.2 dB	19.2 dB
	10^{-3}	22.7 dB	10 dB	**9.8 dB**	-	10 dB	-	10 dB	-
	lowest BER	0.8e-3	0.2e-3	0.2e-3	1.9e-3	**0**	7.2e-3	**0**	9.8e-3
V2I (NLOS) $\Delta v = 10\,km/h$	10^{-2}	19.5 dB	9.7 dB	9.7 dB	-	9.7 dB	-	**9.6 dB**	-
	10^{-3}	-	-	-	-	14.4 dB	-	**13.6 dB**	-
	lowest BER	6.8e-3	3e-3	3.2e-3	15.1e-3	0.5e-3	53.1e-3	**0**	67.5e-3
V2I $\Delta v = 50\,km/h$	10^{-2}	10 dB	**7.6 dB**	**7.6 dB**	7.9 dB	8.7 dB	9.9 dB	9 dB	-
	10^{-3}	23.4 dB	**10 dB**	**10 dB**	-	10 dB	-	11.6 dB	-
	lowest BER	0.8e-3	0.3e-3	0.3e-3	2e-3	0.1e-3	7.7e-3	**0**	10.2e-3
V2I (NLOS) $\Delta v = 50\,km/h$	10^{-2}	19.1 dB	**9.7 dB**	**9.7 dB**	-	9.8 dB	-	9.8 dB	-
	10^{-2}	-	-	-	-	**14.5 dB**	-	**14.5 dB**	-
	lowest BER	6.3e-3	2.5e-3	2.6e-3	13.7e-3	0.3e-3	53.1e-3	**0**	67.6e-3
V2I $\Delta v = 100\,km/h$	10^{-2}	10 dB	**8.2 dB**	8.4 dB	8.3 dB	9.5 dB	10 dB	13.5 dB	-
	10^{-3}	-	**12.4 dB**	12.7 dB	-	14.4 dB	-	-	-
	lowest BER	1.1e-3	**0.5e-3**	**0.5e-3**	2.4e-3	0.3e-3	7.9e-3	4.7e-3	10.3e-3
V2I (NLOS) $\Delta v = 100\,km/h$	10^{-2}	19.6 dB	**9.9 dB**	**9.9 dB**	-	11.1 dB	-	14.6 dB	-
	10^{-3}	-	-	-	-	**19.9 dB**	-	-	-
	lowest BER	7.4e-3	3.5e-3	3.8e-3	15.4e-3	**0.8e-3**	54.6e-3	40e-3	69e-3
V2I $\Delta v = 260\,km/h$	10^{-2}	10 dB	**7.8 dB**	7.9 dB	8 dB	9.1 dB	9.8 dB	9.8 dB	-
	10^{-3}	-	**10.9 dB**	11.2 dB	-	12.6 dB	-	20.6 dB	-
	lowest BER	1.1e-3	0.4e-3	0.5e-3	2.2e-3	**0.1e-3**	7.6e-3	0.8e-3	10.1e-3
V2V $\Delta v = 90\,km/h$	10^{-2}	11.4 dB	8.9 dB	9.1 dB	**8.7 dB**	10 dB	10 dB	-	-
	10^{-3}	19.5 dB	**12.5 dB**	13.8 dB	-	-	-	-	-
	lowest BER	0.2e-3	**0.1e-3**	0.3e-3	1.1e-3	1.4e-3	7.5e-3	16.6e-3	10.3e-3
V2V $\Delta v = 160\,km/h$	10^{-2}	11.7 dB	8.9 dB	9 dB	**8.7 dB**	9.9 dB	10 dB	-	-
	10^{-3}	18.9 dB	**11.7 dB**	12.7 dB	-	-	-	-	-
	lowest BER	0.2e-3	**0.1e-3**	0.2e-3	1e-3	1.2e-3	7.4e-3	12.7e-3	10.3e-3

REFERENCES

[1] T. Wang, J. G. Proakis, E. Masry, and J. R. Zeidler, "Performance degradation of OFDM systems due to Doppler spreading," *IEEE Trans. on Wireless Commun.*, vol. 5, no. 6, pp. 1422–1432, 2006.

[2] R. Hadani, S. Rakib, M. Tsatsanis, A. Monk, A. J. Goldsmith, A. F. Molisch, and R. Calderbank, "Orthogonal time frequency space modulation," in *2017 IEEE Wireless Commun. and Netw. Conf. (WCNC)*, pp. 1–6, IEEE, 2017.

[3] R. Hadani, S. Rakib, A. F. Molisch, C. Ibars, A. Monk, M. Tsatsanis, J. Delfeld, A. Goldsmith, and R. Calderbank, "Orthogonal Time Frequency Space (OTFS) modulation for millimeter-wave communications systems," in *2017 IEEE MTT-S Int. Microwave Symp. (IMS)*, pp. 681–683, June 2017.

[4] M. Kollengode Ramachandran and A. Chockalingam, "MIMO-OTFS in High-Doppler Fading Channels: Signal Detection and Channel Estimation," in *2018 IEEE Global Commun. Conf. (GLOBECOM)*, pp. 206–212, Dec 2018.

[5] P. Raviteja, Y. Hong, E. Viterbo, and E. Biglieri, "Practical Pulse-Shaping Waveforms for Reduced-Cyclic-Prefix OTFS," *IEEE Trans. on Vehicular Technol.*, vol. 68, pp. 957–961, Jan 2019.

[6] A. Nimr, M. Chafii, M. Matthe, and G. Fettweis, "Extended GFDM Framework: OTFS and GFDM Comparison," in *2018 IEEE Global Commun. Conf. (GLOBECOM)*, pp. 1–6, Dec 2018.

[7] W. Kozek, "Matched Weyl-Heisenberg expansions of nonstationary environments," 1996.

[8] K. Liu, T. Kadous, and A. M. Sayeed, "Orthogonal time-frequency signaling over doubly dispersive channels," *IEEE Trans. on Inf. Theory*, vol. 50, no. 11, pp. 2583–2603, 2004.

[9] P. Jung and G. Wunder, "WSSUS pulse design problem in multicarrier transmission," *IEEE Trans. on Commun.*, vol. 55, no. 9, pp. 1822–1822, 2007.

[10] W. Kozek and A. F. Molisch, "Nonorthogonal pulseshapes for multicarrier communications in doubly dispersive channels," *IEEE J. on Sel. Areas in Commun.*, vol. 16, pp. 1579–1589, Oct 1998.

[11] T. Zemen, M. Hofer, D. Loeschenbrand, and C. Pacher, "Iterative detection for orthogonal precoding in doubly selective channels," in *2018 IEEE 29th Annual Int. Symp. on Pers., Indoor and Mobile Radio Commun. (PIMRC)*, pp. 1–7, IEEE, 2018.

[12] X. Ma and W. Zhang, "Fundamental limits of linear equalizers: diversity, capacity, and complexity," *IEEE Trans. on Inf. Theory*, vol. 54, no. 8, pp. 3442–3456, 2008.

[13] T. Zemen, M. Hofer, and D. Loeschenbrand, "Low-complexity equalization for orthogonal time and frequency signaling (OTFS)," *arXiv preprint arXiv:1710.09916*, 2017.

[14] A. Pfadler, P. Jung, and S. Stanczak, "Pulse-Shaped OTFS for V2X Short-Frame Commun. with Tuned One-Tap Equalization," in *WSA 2020; 24rd Int. ITG Workshop on Smart Antennas*, pp. 1–6, VDE, 2020.

[15] Z. Průša, P. L. Søndergaard, N. Holighaus, C. Wiesmeyr, and P. Balazs, "The Large Time-Frequency Analysis Toolbox 2.0," in *Sound, Music, and Motion*, LNCS, pp. 419–442, Springer Int. Publishing, 2014.

[16] S. Jaeckel, L. Raschkowski, K. Börner, and L. Thiele, "QuaDRiGa: A 3-D multi-cell channel model with time evolution for enabling virtual field trials," *IEEE Trans. on Antennas and Propag.*, vol. 62, no. 6, pp. 3242–3256, 2014.

[17] R. Hadani and S. S. Rakib, "OTFS methods of data channel characterization and uses thereof," Sept. 13 2016. US Patent 9,444,514.

[18] K. Gröchenig, *Foundations of time-frequency analysis*. Springer Science & Business Media, 2013.

[19] G. Matz, D. Schafhuber, K. Grochenig, M. Hartmann, and F. Hlawatsch, "Analysis, optimization, and implementation of low-interference wireless multicarrier systems," *IEEE Trans. on Wireless Commun.*, vol. 6, no. 5, pp. 1921–1931, 2007.

[20] P. Raviteja, K. T. Phan, and Y. Hong, "Embedded Pilot-Aided Channel Estimation for OTFS in Delay-Doppler Channels," *IEEE Trans. on Vehicular Technol.*, pp. 1–1, 2019.

[21] P. Bello, "Characterization of randomly time-variant linear channels," *IEEE Trans. on Commun. Syst.*, vol. 11, no. 4, pp. 360–393, 1963.

[22] P. Jung, W. Schuele, and G. Wunder, "Robust path detection for the LTE downlink based on compressed sensing," in *14th Int. OFDM-Workshop, Hamburg*, 2009.